Journal of Hazardous Materials 190 (2011) 150–158

Contents lists available at ScienceDirect

Journal of Hazardous Materials

journal homepage: www.elsevier.com/locate/jhazmat

Lung cancer risk in relation to traffic-related nano/ultrafine particle-bound PAHs exposure: A preliminary probabilistic assessment

Chung-Min Liao[a,*], Chia-Pin Chio[a,1], Wei-Yu Chen[a,1], Yun-Ru Ju[a,1], Wen-Hsuan Li[a,1], Yi-Hsien Cheng[a,1], Vivian Hsiu-Chuan Liao[a], Szu-Chieh Chen[b,c], Min-Pei Ling[d]

[a] Department of Bioenvironmental Systems Engineering, National Taiwan University, Taipei 10617, Taiwan, ROC
[b] Department of Public Health, Chung Shan Medical University, Taichung 40242, Taiwan, ROC
[c] Department of Family and Community Medicine, Chung Shan Medical University Hospital, Taichung 40242, Taiwan, ROC
[d] Department of Health Risk Management, China Medical University, Taichung 40202, Taiwan, ROC

ARTICLE INFO

Article history:
Received 15 December 2010
Received in revised form 21 February 2011
Accepted 5 March 2011
Available online 12 March 2011

Keywords:
Polycyclic aromatic hydrocarbons
Nanoparticles
Particulate matter
Lung cancer
Population attributable fraction
Risk assessment

ABSTRACT

Exposures to carcinogenic polycyclic aromatic hydrocarbons (PAHs) have been linked to human lung cancer. The purpose of this study was to assess lung cancer risk caused by inhalation exposure to nano/ultrafine particle-bound PAHs at the population level in Taiwan appraised with recent published data. A human respiratory tract model was linked with a physiologically based pharmacokinetic model to estimate deposition fraction and internal organic-specific PAHs doses. A probabilistic risk assessment framework was developed to estimate potential lung cancer risk. We reanalyzed particle size distribution, total-PAHs, particle-bound benzo(*a*)pyrene (B[*a*]P) and PM concentrations. A dose–response profile describing the relationships between external B[*a*]P concentration and lung cancer risk response was constructed based on population attributable fraction (*PAF*). We found that 90% probability lung cancer risks ranged from 10^{-5} to 10^{-4} for traffic-related nano and ultrafine particle-bound PAHs, indicating a potential lung cancer risk. The particle size-specific *PAF*-based excess annual lung cancer incidence rate due to PAHs exposure was estimated to be less than 1 per 100,000 population, indicating a mild risk factor for lung cancer. We concluded that probabilistic risk assessment linked *PAF* for limiting cumulative PAHs emissions to reduce lung cancer risk plays a prominent role in future government risk assessment program.

1. Introduction

Laboratory experiments, field observations, and epidemiological studies all link atmospheric polycyclic aromatic hydrocarbons (PAHs), a carcinogenic chemical, to increases in human exposure risks, suggesting that atmospheric PAHs have strong association with human lung cancer [1–10].

Lung cancer has been ranked as the second and first leading causes of cancer death in Taiwan males and females, respectively. The age-adjusted mortality rate for lung cancer was nearly 38 per 100,000 among males and 17 among females in 2007 [11]. In Taiwan region, several significant contributor to PAHs sources had been sampled such as stationary industrial combustion of steel and iron industries [12] with a mean total-PAHs concentrations measured to be 1020 $\mu g\,m^{-3}$; and traffic vehicles exhaust of motorcycle [13] and highway toll station [14] with a mean total-PAHs concentrations ranged from 8280 to 12,300 $ng\,m^{-3}$. Fang et al. [15–17] indicated that mean total PAHs levels at industrial, urban, and rural area in central Taiwan region ranged from 1232 to 1650, 700 to 1740, and 610 to 831 $ng\,m^{-3}$, respectively.

Nanoparticles have been previously shown to induce lung inflammation by stimulating pulmonary epithelial cells to produce proinflammatory cytokines and by causing endothelial cells to express leukocyte adhesion molecules and recruit circulating leukocytes [18–22]. Recently, the issues of health effects linked to fine particles-bound PAHs keeps growing. Bocskay et al. [23] indicated that the newborn babies of New York City mothers exposed to $PM_{2.5}$ ($D_p \leq 2.5\,\mu m$) containing higher levels of PAHs had more chromosomal damage that can later lead to cancer than did the babies of mothers with lower PAH exposures.

Lin et al. [6] reported the relevant measurements of nanopartcile-bound PAHs in a heavily trafficked roadside in a city in southern Taiwan. Lin et al. [6] indicated that the mean content of particle-bound total-PAHs/B[*a*]P_{eq}s (benzo(*a*)pyrene equivalent) and PAH/B[*a*]P_{eq}-derived carcinogenic potency followed the order of nano ($0.01\,\mu m < D_p < 0.056\,\mu m$) > ultrafine

* Corresponding author. Tel.: +886 2 2363 4512; fax: +886 2 2362 6433.
E-mail addresses: cmliao@ntu.edu.tw, cmliao@ccms.ntu.edu.tw (C.-M. Liao).
[1] These authors contributed equally to this work that was initiated in the Spring 2010 Class "Simulation and Computation of Biosystems."

0304-3894/$ – see front matter © 2011 Elsevier B.V. All rights reserved.
doi:10.1016/j.jhazmat.2011.03.017

($0.01\,\mu m < D_p < 0.10\,\mu m$) > fine ($PM_{2.5}$) > coarse ($PM_{2.5-10}$). They concluded that traffic-related nano and ultrafine particles are possibly cytotoxic. Kawanaka et al. [9] indicated that ultrafine particles were shown to contribute as much as 23–30% and 10–16% to PAH deposition in the alveolar for the roadside and suburban atmosphere, respectively, implicating that ultrafine particles are significant contributors to the deposition of PAHs into the alveolar region of the lung.

The significant variations in respiration rate and genetic susceptibility among populations, and its relationship to PAHs exposure risk, suggests probabilistic lung cancer risk assessment should incorporate this variability [10]. Recently, population attributable fraction (*PAF*) concept, taking into account variability in respiration rate and genetic susceptibility, was applied successfully to address the global disease burden caused by multiple risk factors [24,25] and the relationship between ambient PAH exposure and lung cancer in China [10]. Parsimoniously, *PAF* can be defined as $PAF \equiv (R - R_0)/R$ where R is the lifetime cancer risk of the total population and R_0 is the lifetime cancer risk in the population after elimination of the exposure to carcinogens considered [26].

Numerous mathematical models for predicting PM deposition and organic chemicals distribution in human respiratory tract (HRT) and other tissues have been developed in a decade [27–32]. Chen et al. [29] and Liao and Chen [32] developed a complete and realistic PM exposure model for HRT containing airflow dynamic, physiological, lung morphological, and dose cumulated submodels. Dennison et al. [30] and Clewell et al. [31] used physiologically based pharmacokinetic (PBPK) models to describe the absorption, distribution, metabolism, and excretion of individual chemical (perchloroethylene) and chemical mixtures (gasoline) in human.

Currently, no information on the potential health risk assessment of lung cancer related to environmental nano/ultrafine particle-bound PAH is available in Taiwan region. Therefore, in light of the mutagenicity, carcinogenicity and ubiquity of some PAHs in the atmosphere, the setting of air quality standards and guidelines to limit human exposure should be of primary concern for public health policy. However, setting scientifically based limit values is complicated, owing to the difficulties in interpreting heterogeneous experimental and epidemiological findings [7,8].

Despite much recent progress in our understanding of source attribution, emission factors and regulation of PAHs [7], current risk assessment models based on parameterization of laboratory experiments cannot fully explain the magnitude of nano/ultrafine particle-bound PAHs induced lung cancer risk. Here we integrated *PAF*-based dose–response relationships to better characterize the lung cancer caused by inhalation exposure to nano/ultrafine particle-bound PAHs.

The objective of this study was fourfold: (1) to assess the lung cancer risk caused by inhalation exposure to size-specific environmental PAHs, emphasizing on nano/ultrafine particle-bound PAHs, at the population level in Taiwan appraised with recent published data, (2) to estimate the deposition fractions in different human respiratory tract regions by using the HRT model, (3) to utilize a PBPK model to estimate the time-dependent internal organic-specific PAHs doses, and (4) to integrate a probabilistic risk assessment framework and the *PAF*-based dose–response profile to estimate excess lung cancer incidence rate in Taiwan population.

2. Materials and methods

2.1. Study data

We reanalyzed quantitatively the particle size distribution, total-PAH, particle-bound B[*a*]P_{eq} and PM concentrations with sizes of nano, ultrafine, fine, from recent published data. Thanks to Lin et al. [6] who have provided the remarkable dataset related to traffic-related PAHs in southern Taiwan. The PAHs data give us the opportunity to test all theoretical considerations of nano/ultrafine particle-bound PAHs exposure effects and quantify its strength.

Table 1
Study data of size-specific concentrations of PM, total PAHs, and B[*a*]P_{eq} adopted from Lin et al. [6].

Particle size	PM ($\mu g\,m^{-3}$)	$\sum$PAHs ($ng\,m^{-3}$)	B[*a*]P_{eq} ($ng\,m^{-3}$)
Nano ($PM_{0.01-0.056}$)	13.1 ± 4.48[a]	18.7 ± 4.95	1.44 ± 0.539
Ultrafine ($PM_{0.01-0.1}$)	16.5 ± 3.59	21.3 ± 5.51	1.69 ± 0.589
Fine ($PM_{0.01-2.5}$)	93 ± 30.6	44.6 ± 18.6	3.53 ± 0.924
Coarse ($PM_{2.5-10}$)	47.1 ± 23.5	9.49 ± 6.07	0.662 ± 0.181

[a] Mean ± SD.

Briefly, Lin et al. [6] have chosen a heavily trafficked roadside in a city of southern Taiwan as the sample site to collect all of the atmospheric PM samples by using collectors of a MOUDI and a nano-MOUDI. They divided deliberately the PMs into four size groups: nano ($PM_{0.01-0.056}$: $0.01\,\mu m < D_p < 0.056\,\mu m$), ultrafine ($PM_{0.01-0.1}$: $0.01\,\mu m < D_p < 0.10\,\mu m$), fine ($PM_{2.5}$), and coarse ($PM_{2.5-10}$).

Of 15 PAH compounds of middle (4-ring) and high (5-/6-/7-ring) molecular weights were identified and quantified by a gas chromatograph/mass spectrometer (GC/MS) and a mass-selective detector: four 4-ring (fluoranthene, pyrene, benzo(*a*)anthracene, and chrysene), six 5-ring (cyclopenta(*c*,*d*)pyrene, benzo(*b*)fluoranthene, benzo(*k*)fluoranthene, benzo(*e*)pyrene, benzo(*a*)pyrene, and perylene), four 6-ring (indeno(1,2,3-*cd*)pyrene, dibenzo(*a*,*h*)anthrance, benzo(*b*)chrycene, and benzo(ghi)perylene), and one 7-ring (coronene). The limits of detection of GC/MS ranged from 0.023 to 0.106 ng, whereas the limits of quantification ranged from 0.122 to 0.561 $ng\,m^{-3}$ for the identified 15 PAH compounds. The samplings were performed during August 2004–May 2006. The daily sampling time was from 07:00 to 22:00 (15 h).

Table 1 summarizes the size-specific measured concentrations of PM, total PAHs, and B[*a*]P_{eq}.

2.2. Exposure models

We divided human respiratory tract (HRT) into five major compartments from the suggestion of ICRP66 [27]: (i) the nasal passage (ET1), comprising the anterior nose and the posterior nasal passages; (ii) the pharynx (ET2), comprising the larynx and mouth; (iii) the bronchial region (BB), comprising the airway from the trachea, main bronchi, and intrapulmonary bronchi; (iv) the bronchiolar region (bb), comprising the bronchioles and terminal bronchioles; and (v) the alveolar-interstitial region (AI), comprising the airway from the respiratory bronchioli through the alveolar sacs.

Followed by the principle of mass balance, the dynamic equations of inspiratory oral cavity varying with particle size range k and time t to each regional compartment are given by a state-space realization form of a linear dynamic representation [29,33] (Appendix A). The reference values for anatomical and physiological parameters, including volumes, breathing rates, transfer coefficients, and clearance rate, are taken from ICRP66 [27]. More details for HRT model developments and constructions have been described in elsewhere [29,33].

For simulating the inhalation pharmacokinetics of PAH, we used a basic human compartment structure that has been previously used in many PBPK models [34,35]. The tissue compartments included in the model were: alveolus, lung, richly perfused tissues (brain, gut, kidney, spleen, and heart), fat, slowly perfused tissues (bone, muscle, and skin), and liver. Each tissue compartment was interconnected by arterial and venous blood (Appendix B). The mathematical descriptions of pharmacokinetic processes

employed in the PBPK model were provided in Appendix B. The physiological and biochemical parameters were listed in Appendix C (Table C1). The tissue:blood partition coefficients were calculated based on the published data [36,37]. The metabolic constants were determined by using the allometric scaling for interspecies extrapolation [38].

2.3. Dose–response models

To construct a dose–response profile describing the relationships between external B[*a*]P$_{eq}$ concentration and lung cancer risk response, the population attributable fraction (*PAF*) concept that builds on past well-defined models [10,26] is used. Specifically, environmental PAHs exposure-deduced *PAF* distribution used to estimate lung cancer risk has the form as [10,26],

$$PAF = \frac{rr(C_{\mathrm{BaP,e}}) - 1}{rr(C_{\mathrm{BaP,e}})} \quad (1)$$

$$rr(C_{BaP,e}) = 1 + \{URR^{(((IR/BW)/IR_{\mathrm{m}})\times C_{\mathrm{BaP,e}}\times(70/100))} - 1\} \times sus, \quad (2)$$

where $rr(C_{\mathrm{BaP,e}})$ is the external B[*a*]P$_{eq}$ concentration $C_{\mathrm{BaP,e}}$ associated relative risk that can be estimated from a dose–response model developed by Armstrong et al. [4], *URR* is the unit relative risk at a benchmark of 100 μg m^{-3}-year of B[*a*]P exposure [4], *IR* is the respiration rate (m^3 d^{-1}), *BW* is the body weight (kg), IR_{m} is the mean value of per unit body weight respiration rate (m^3 d^{-1} kg^{-1}), *sus* is the genetic susceptibility [10], and 70 is the lifelong exposure period (year). Here *IR*, *BW*, $C_{\mathrm{BaP,e}}$, and *sus* were treated probabilistically.

A joint probability technique can be used to link probability distributions of external B[*a*]P$_{eq}$ concentration ($P(C_{\mathrm{BaP,e}})$) and *PAF* ($P(PAF)$) to construct a dose–response model as

$$P(PAF|C_{\mathrm{BaP,e}}) = P(C_{\mathrm{BaP,e}}) \times P(PAF), \quad (3)$$

where $P(PAF|C_{\mathrm{BaP,e}})$ is a conditional probability distribution used to represent the relationships between *PAF* and external B[*a*]P$_{eq}$ concentration.

Here we used a three parameters Hill equation model to optimal fit epidemiological data to reconstruct a dose–response profile describing the relationship between *PAF* and external B[*a*]P$_{eq}$ concentration ($C_{\mathrm{BaP,e}}$) as

$$PAF = \frac{PAF_{\max}}{1 + (\mathrm{EC50}/C_{\mathrm{BaP,e}})^n} \quad (4)$$

where $PAF_{\max}$ is the maximum *PAF*, EC50 is the external B[*a*]P$_{eq}$ concentration giving half-maximum *PAF*, and *n* is the Hill coefficient reflecting the overall shape of the curve and cooperativity.

2.4. Lung cancer risk models

We combined the exposure analysis with the analysis of biological effects expected at various concentrations to calculate individual risk. We employed the joint probability function to describe the probability of an external concentration and internal dose exceeding a concentration that resulted in particular magnitude of biological effect. This results in a joint probability function or exceedance risk profile as

$$R_{C_{\mathrm{BaP,e}}} = P(C_{\mathrm{BaP,e}}) \times P(PAF|C_{\mathrm{BaP,e}}), \quad (5)$$

where $R_{C_{\mathrm{BaP,e}}}$ is the risk at the specific external concentration of B[*a*]P$_{eq}$, $P(C_{\mathrm{BaP,e}})$ is the probability density function of measured $C_{\mathrm{BaP,e}}$, and $P(PAF|C_{\mathrm{BaP,e}})$ is the conditional cumulative distribution functions given ambient concentration of B[*a*]P$_{eq}$.

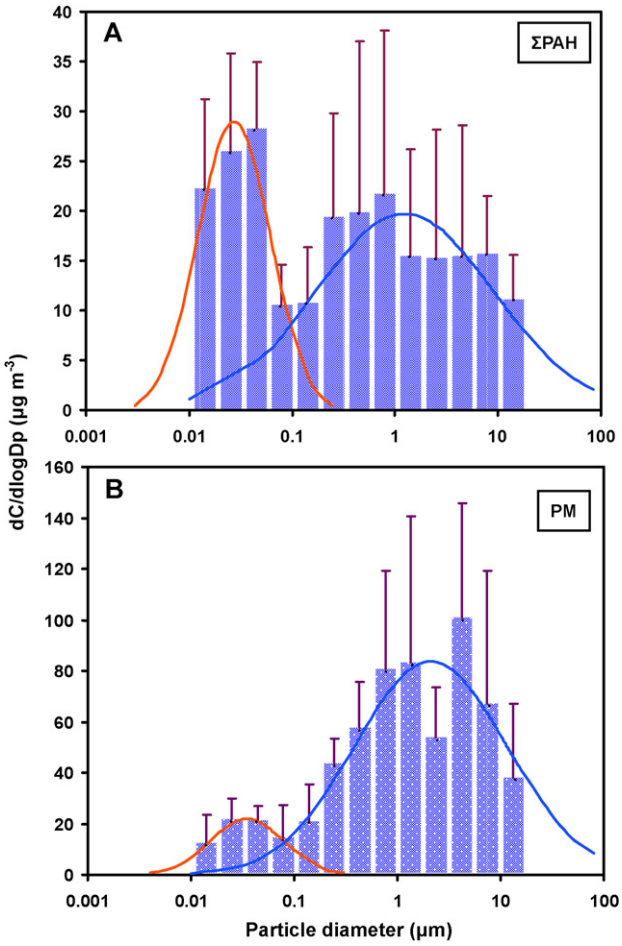

Fig. 1. Model fitting of (A) ∑PAH and (B) PM size distributions to study data. Lines with red and blue colors are presented as fine and coarse modals, respectively.

2.5. Uncertainty and data analysis

Optimal statistical models were selected on the basis of least squared criterion from a set of generalized linear and nonlinear autoregression models provided by TableCurve 2D packages (AISN Software Inc., Mapleton, OR, USA) fitted to the study data. A value of $p < 0.05$ was judged significant. To quantify the uncertainty and its impact on the estimation of expected risk, a Monte Carlo (MC) technique was implemented. A MC simulation was also performed with 10,000 iterations to generate 2.5- and 97.5-percentiles as the 95% CI for all fitted models. The Crystal Ball® software (Version 2000.2, Decisionerring, Inc., Denver, Colorado, USA) was employed to implement MC simulation. The MATLAB® software (The Mathworks Inc., MA, USA) was used to perform the simulations of HRT and PBPK models.

3. Results

3.1. Quantitative analysis of data

A bimodal distribution was found for size distributions of total APHs and PM measurements (Fig. 1). The lognormal (LN) distribution was successfully fitted to the size distribution measurements of total PAHs with a geometric mean (gm) 0.03 μm and a geometric standard deviation (gsd) 2.26 for ultrafine size range (LN(0.03 μm, 2.26), $r^2 = 0.96$) and LN(1.23 μm, 7.27) for fine size range ($r^2 = 0.63$) (Fig. 1A). On the other hand, for PM size distribution, the optimal fits were estimated to be LN(0.03 μm, 2.27) for ultrafine size

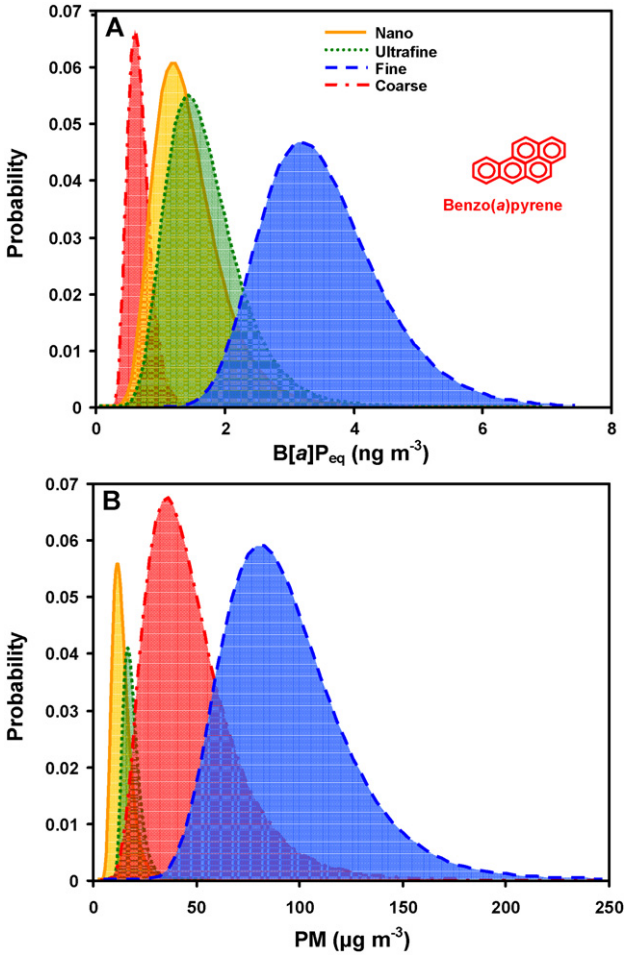

Fig. 2. The probabilities of (A) B[*a*]P_{eq} and (B) PM mass concentrations with nano (solid line), ultrafine (point line), fine (dash line), and coarse (dash with point line) size fractions. All the posterior probabilities are estimated from prior distribution of the measured data [6].

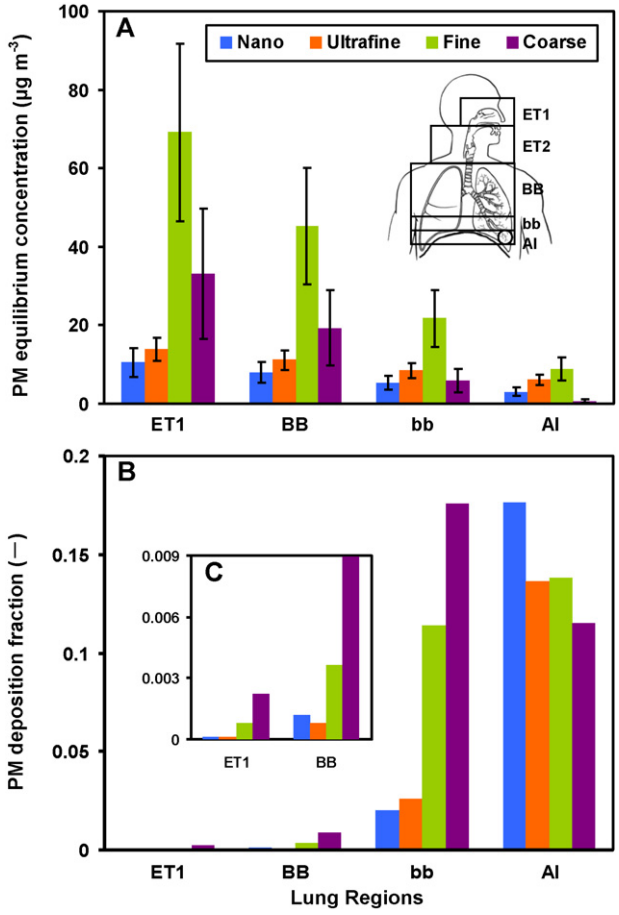

Fig. 3. The PM (A) equilibrium concentrations and (B) deposition fractions for nano, ultrafine, fine, and coarse particles in different human lung regions estimated by human respiratory tract (HRT) model. (C) The enhanced plot of the PM deposition fractions estimated in ET1 and BB lung regions. More details of the five compartments of human lung regions are showed in Appendix A.

range (r^2 = 0.99) and LN(2.10 μm, 5.42) for fine size range (r^2 = 0.78) (Fig. 1B).

The optimal fitted probability distributions of size-specific B[*a*]P_{eq} were estimated to be LN(1.35 ng m^{-3}, 1.44), LN(1.60 ng m^{-3}, 1.40), LN(3.41 ng m^{-3}, 1.30), and LN(0.64 ng m^{-3}, 1.31) for nano, ultrafine, fine, and coarse sized particles, respectively (Fig. 2A). Meanwhile, for PM concentrations, the best-fitted distributions were found to be LN(12.36 μg m^{-3}, 1.40), LN(16.14 μg m^{-3}, 1.24), LN(88.33 μg m^{-3}, 1.38), and LN(42.11 μg m^{-3}, 1.60) for nano, ultrafine, fine, and coarse sized particles, respectively (Fig. 2B).

3.2. HRT PM deposition and target organ B[*a*]P_{eq} doses

Because the airborne PM concentrations within the four regions reached the steady state in 5–10 s for all the size ranges, it is more important to understand the size-specific equilibrium PM concentration than the dynamics of airborne PM in HRT. Generally, ET1 experienced the largest PM equilibrium concentration for all size range than those of BB, bb, and AI regions (Fig. 3A). Specifically, fine PMs had the highest concentration deposited in all lung regions with 70 ± 20 (mean ± sd) μg m^{-3} in ET1, 45 ± 15 μg m^{-3} in BB, 20 ± 10 μg m^{-3} in bb, and 10 ± 5 μg m^{-3} in AI regions (Fig. 3A).

Noted, however, that coarse PM concentrations were unlikely to have reached in deeper regions of bb and AI. A comparison of the equilibrium PM concentrations in four regions indicated that PM concentrations are much lower in the deeper AI region, suggesting that the deposition effect makes PM no longer airborne especially in larger size ranges (Fig. 3A). In view of PM deposition fraction, larger size PM experienced higher deposition fraction in upper lung regions ET1, BB, and bb, whereas in deep region of AI, nano-sized PM gave a much higher deposition fraction than those of ultrafine, fine, and coarse PMs (Fig. 3B).

Fig. 4 shows the simulated time-course concentrations of B[*a*]P_{eq} in human tissues following inhalation exposure to nano- and ultrafine particle-bound PAHs. Peak exposure (12 h d^{-1} on 50 consecutive days (Fig. 4B)) was clearly reflected by fluctuating concentrations in human tissues which increased with duration of exposure and reached steady-state. The highest nano and ultrafine B[*a*]P_{eq} concentrations were observed in fat with an order of magnitude of 10^{-7} mg L^{-1}, followed by richly perfused tissues, slowly perfused tissues, liver, and lung, indicating that B[*a*]P is the highly lipophilic compound and accumulates easily in human (Fig. 4A and C). Moreover, the fat tissue has the highest concentration, whereas the lung and liver tissues experienced the lowest concentration which was attributable to the properties such as lipophilicity and metabolic clearance of tissues.

3.3. Dose–response analysis

To obtain the *PAF* cumulative probability distribution, the probability distributions of ambient B[*a*]P_{eq} concentration ($C_{BaP,e}$), genetic susceptibility (*sus*), respiratory rate (*IR*), and body weight

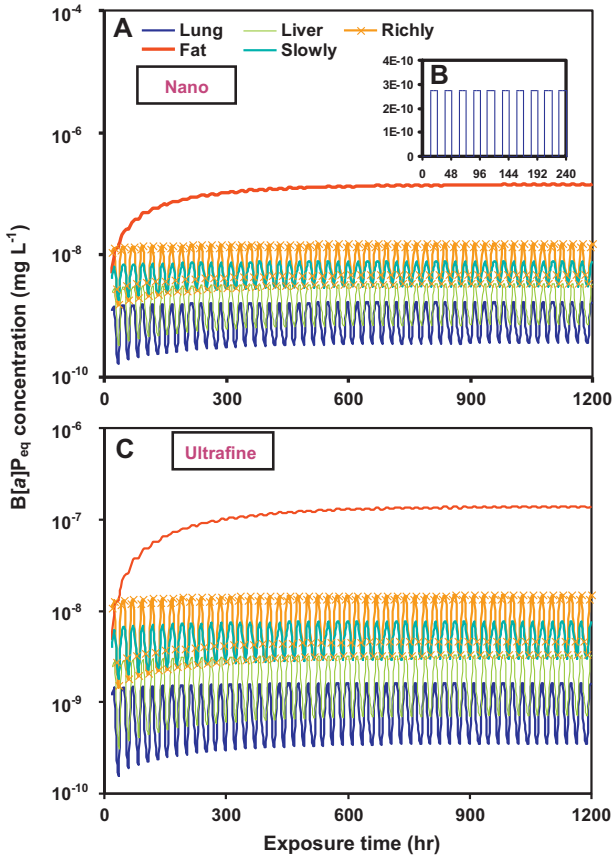

Fig. 4. (A) Internal B[*a*]P_{eq} concentration in human tissues for human exposed to nano-sized particle-bound PAHs by using PBPK model. (B) The 12 h:12 h exposure pattern of B[*a*]P consumption from inhaled particle as PBPK model input. (C) The same simulation but exposed to ultrafine-sized particle-bound PAHs.

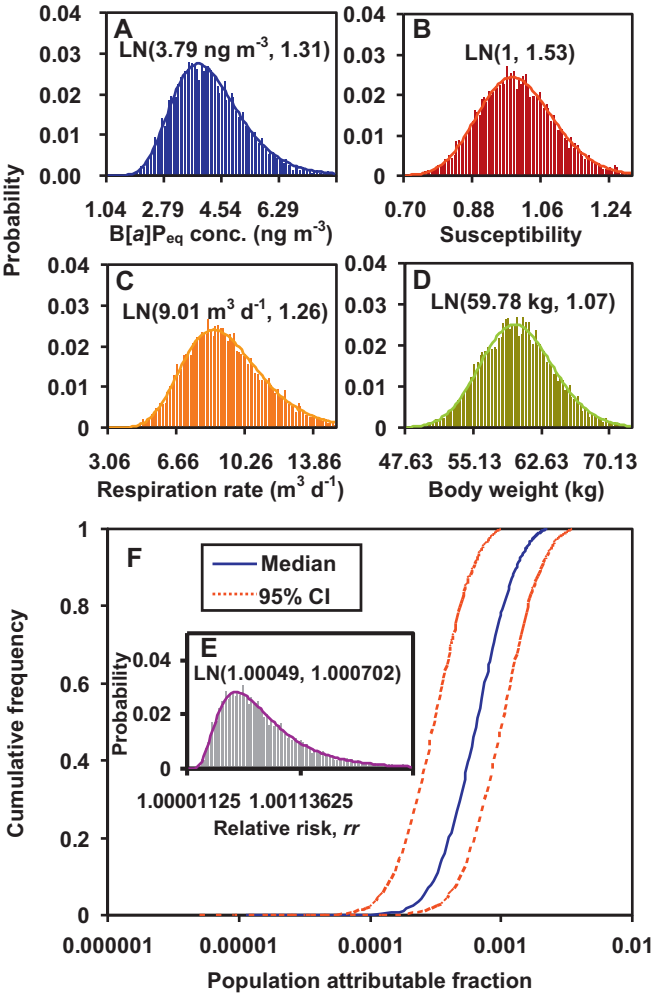

Fig. 5. The parameters used for population attributable fraction (*PAF*) based dose–response model. The probability distributions of (A) ambient B[*a*]P_{eq} concentration, (B) genetic susceptibility, (C) respiratory rate, (D) body weight, and (E) selected relative risk are model inputs. (F) The estimated median (solid line) with 95% CIs (dash lines) of cumulative frequency curves upon varied *PAF* intensities.

(*BW*) appeared in relative risk (*rr*) relations (Eqs. (1) and (2)) have to be estimated (Fig. 5A–D). The resulted relative risk *rr* had a fitted lognormal distribution with a gm of 1.00049 and a gsd of 1.000702 based on a unit relative risk (*URR*) of 1.30 that was adopted from Armstrong et al. [4] for Asia continent (Fig. 5E). Fig. 5F presents the estimated cumulative frequency of *PAF* with variability in respiration rate and genetic susceptibility for lung cancer induced by inhalation exposure to ambient PAHs.

Based on the joint probability technique (Eq. (3)), a linkage of external B[*a*]P_{eq} concentration and *PAF* cumulative distribution can then be obtained successfully to present the dose–response profile describing the relationships between ambient B[*a*]P_{eq} level and *PAF* (Fig. 6A and B). A fit functionality was derived from MC modeling of a Hill-type equation (Eq. (1)) to represent mathematically the *PAF*–B[*a*]P_{eq} dose–response model with cooperativity of Hill coefficient $n = 2.61 \pm 0.5$, maximum response $PAF_{max} = 4.30 \times 10^{-3}$, and half-maximum response of B[*a*]P_{eq} *EC*50 = 7.73 (95% CI: 7.04–8.42) ng m^{-3} ($r^2 = 0.99$) (Fig. 6A and B).

3.4. Lung cancer risk and excess incidence rate estimates

The particle size-specific exceeding thresholds for the probabilities of lung cancer at risks of 0.1, 0.5, and 0.9 induced by inhalation exposure of PAHs are summarized in Table 2. Our results indicated that 50% or more probability (risk = 0.5) of average lung cancer induced by traffic-related PAH exposure were estimated to be 4.4×10^{-5} for nano-, 6.65×10^{-5} for ultrafine-, 4.45×10^{-4} for fine-, and 6.21×10^{-6} for coarse-sized particles (Fig. 7, Table 2).

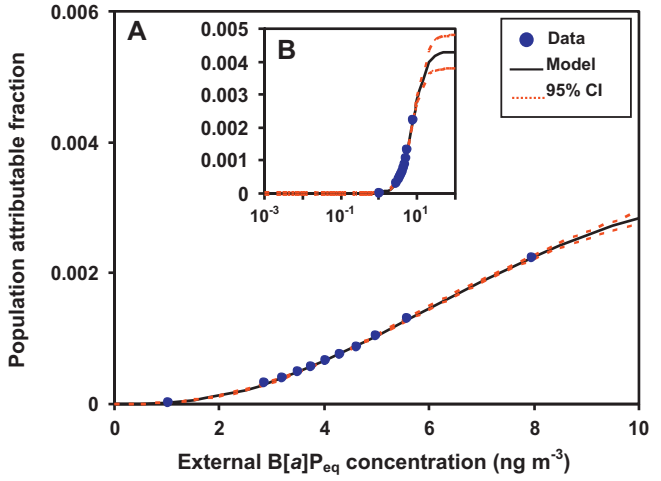

Fig. 6. The reconstructed population attributable fraction (*PAF*)–B[*a*]P_{eq} dose–response function. The curves estimated with exposure to (A) the external B[*a*]P_{eq} ranged from 0 to 10 ng m^{-3}, and (B) the external B[*a*]P_{eq} greater than 10 ng m^{-3}.

Table 2
Population attributable fraction-based lung cancer rexceedance risk estimates for different particle sizes at 90%, 50%, and 10% probability exposed to environmental B[*a*]P_{eq} in which values of 95% confidence interval (CI) are given in parentheses.

Particle size	Exceedance risk		
	0.9	0.5	0.1
Nano	1.32×10^{-5} (8.39×10^{-6}–2.05×10^{-5})	4.40×10^{-5} (2.99×10^{-5}–6.30×10^{-5})	1.36×10^{-4} (9.97×10^{-5}–1.81×10^{-4})
Ultrafine	2.15×10^{-5} (1.41×10^{-5}–3.24×10^{-5})	6.65×10^{-5} (4.65×10^{-5}–9.29×10^{-5})	1.87×10^{-4} (1.41×10^{-4}–2.44×10^{-4})
Fine	2.00×10^{-4} (1.51×10^{-4}–2.58×10^{-4})	4.45×10^{-4} (3.59×10^{-4}–5.36×10^{-4})	8.94×10^{-4} (7.75×10^{-4}–9.97×10^{-4})
Coarse	2.52×10^{-6} (1.45×10^{-6}–4.30×10^{-6})	6.21×10^{-6} (7.77×10^{-6}–1.00×10^{-5})	1.47×10^{-5} (9.35×10^{-6}–2.32×10^{-5})

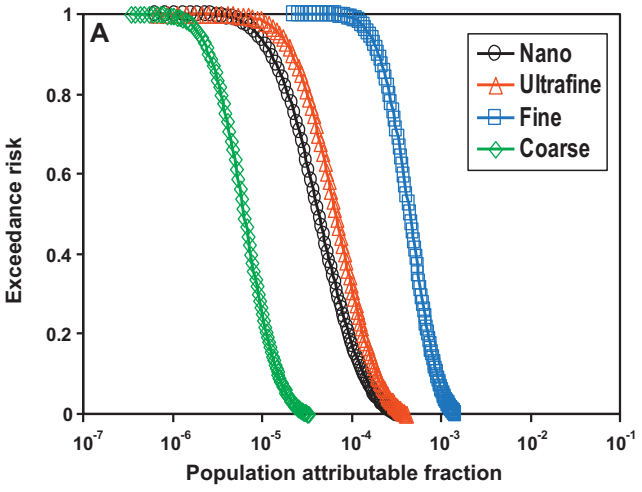

Fig. 7. The exceedance risk estimates based on population attributable fraction (*PAF*) intensities for exposure to nano (circle), ultrafine (triangle), fine (square), and coarse (diamond) particles-bound PAHs.

This finding also revealed that the lung cancer risks induced by nano/ultrafine particle-bound PAHs were significantly higher than those of coarse particle-bound PAHs. Under most conservative regulation program, an exceedence risk fall within range of 10^{-6}–10^{-4} indicates potential health risk. Our results indicate that 90% probability lung cancer risks have orders of magnitude ranging from 10^{-5} to 10^{-4} for traffic-related nano and ultrafine particle-bound PAHs, indicating a potential lung cancer risk (Table 2).

To estimate the excess annual lung cancer incidence rate caused by PAHs exposure in Taiwan region, the present derived Hill-based *PAF*–B[*a*]P_{eq} dose–response model (Fig. 6) was used. The predicted excess annual lung cancer incidence rate caused by PAHs exposure can be calculated by multiplying the actual annual lung cancer incidence rate by the *PAF* estimates shown in Fig. 6. Based on a 9-year averaged actual annual lung cancer incidence rate of 26.62 per 100,000 population in Taiwan region during 1999–2007 [11], the particle size-specific *PAF*-based excess annual lung cancer incidence rate due to PAHs exposure can be predicted (Table 3). Table 3 indicates that the *PAF*-based excess annual lung cancer incidence rate estimates are much less than 1 per 100,000 population, indicating a mild risk factor for lung cancer.

4. Discussion

4.1. Exposure and effect modeling

This study shows that the geometric mean concentrations of B[*a*]P_{eq} were estimated to be 1.35 ng m^{-3} for nano and 1.60 ng m^{-3} for ultrafine particles, that all violate the World Health Organization (WHO) guideline for B[*a*]P_{eq} in ambient air of 1 ng m^{-3} [7]. Meanwhile, larger size PM experienced higher deposition fraction in upper lung regions of ET1, BB, and bb, whereas in deep region of AI, nano-sized PM gave a much higher deposition fraction than those of ultrafine, fine, and coarse PMs. Our results are consistent with most of the research published to date [9,22]. Moreover, the highest nano and ultrafine B[*a*]P_{eq} concentrations were observed in fat tissue with an order of magnitude of 10^{-7} mg L^{-1}, followed by richly perfused tissues, slowly perfused tissues, liver, and lung, indicating that B[*a*]P is the highly lipophilic compound and accumulates easily in human.

In this study, a population attributable fraction (*PAF*) concept was applied to address the relationship between PAHs exposure and lung cancer by taking into account the variation in exposure concentration, respiration rate, body weight, and genetic susceptibility. A Hill-type equation representing the *PAF*–B[*a*]P_{eq} dose–response model was constructed to estimate lung cancer risk and excess lung cancer incidence rate. In view of fine particle-bound PAHs, estimated geometric mean B[*a*]P_{eq} concentration was 3.41 ng m^{-3} with corresponding *PAF* of 0.05% and predicted excess annual lung cancer incidence rate of 0.013 per 100,000 population.

From a conservatism point of view, this study indicates that traffic-related nano and ultrafine particle-bound PAHs are likely to pose potential lung cancer risk. This study thus suggests that an increased risk of lung cancer at the highest exposure levels of fine particle-bound PAHs is alarming. However, the model predicted excess annual lung cancer incidence rate varied between 0.0002 and 0.013 per 100,000 population, indicating a mild risk factor for lung cancer in southern Taiwan region.

The carcinogenic risk assessment for PAHs remains difficult, particularly due to the very high number of these compounds (in the hundreds) present in mixtures to which the general population may be exposed, as well as due to the possible contemporary presence of other risk factors and to possible synergistic and/or antagonistic effects. The choice of B[*a*]P as the reference compound to develop the potency equivalency factor (PEF) was presently questioned [39]. Due to the limited number of dose–response data on carcinogenicity [8], and depending on the exposure route (intratracheal administration, intrapulmonary injection, and so on), different PEFs can be obtained. For example, the PEF value used for DB[*a*,*h*]A was 1.0 [6]. This value may underestimate the relevance of this compound, because other authors claimed a PEF of 5.0 [40]. Noted, however, that the B[*a*]P_{eq} concentrations used for this calculation represent an external exposure estimation of carcinogenic compounds and not the effective active concentration at the lung level.

Recently, human health risk assessments have been frequently based on the biologically effective dose rather than the ambient exposure level [8,30]. Taking physiological and biochemical characteristics into account in exposure models can provide true internal doses of chemicals that would correlate more accurately with toxicity in human than that developed solely on external exposure. Considering the prevalence of PAHs in environment and their known carcinogenic potential, it is noted that PBPK modeling on this class of chemicals has been fairly limited.

The following points may give the explanations: (1) PAH exposure often involves exposure to mixtures of PAHs and other chemicals [6]; (2) exposures are typically to low levels of PAHs, exacerbating the difficulties associated with low-level extrapolation from high-level models [41]; (3) at least some of the airborne

Table 3
Predicted *PAF*-based particle size-specific excess annual lung cancer incidence rates due to environmental PAH exposure based on a 9-year averaged actual annual lung cancer incidence rate of 26.62 per 100,000 population during 1999–2007 in Taiwan region.

Particle size	B[*a*]P$_{eq}$ (ng m^{-3})	Model predicted *PAF*	Predicted *PAF*-based excess annual lung cancer incidence rate (per 100,000 population)
Nano ($PM_{0.01-0.056}$)	1.44 ± 0.539	3.37×10^{-5}	0.0009
Ultrafine ($PM_{0.01-0.1}$)	1.69 ± 0.589	5.62×10^{-5}	0.0015
Fine ($PM_{0.01-2.5}$)	3.53 ± 0.924	5.06×10^{-4}	0.013
Coarse ($PM_{2.5-10}$)	0.662 ± 0.181	7.03×10^{-6}	0.0002

chemical present is adsorbed to surfaces of particles, complicating the assumption of equilibrium between ambient concentrations and the concentration in lung blood [42]; and (4) dermal exposure is also an important route of exposure [10]. However, combining physiologically based pharmacokinetic aspects with quality data can help us enhance exposure assessment for PAHs.

4.2. Limitations and implications

Mode-of-action of a compound has occasionally been considered in risk assessments, either to help in the determination of the particular carcinogenic effect seen in humans or to support the estimation of acceptable levels for human exposures [42]. Information on the carcinogenic mode-of-action in each target tissue becomes more important. Mechanistic exposure models can provide a valuable insight that considers human variability for risk assessment. An arising of human variability is from a variety of sources, including different activity levels altering physiological parameters and metabolizing enzymes [43–45]. It is believed that it would be interesting to explore mode-of-action information and human variability in the future studies.

This study did not perform the experimental work. Therefore, the limitation of this study is the data sources that we adopted to interpret and verify our results. Yet, there are a number of areas in which further research could reduce the uncertainties and limit the variability in this study. Among these are three areas that offer an opportunity for the most useful research. First, there is a need to conduct a more extensive characterization of the distribution of exposures within given population groups. This would require the collection of more detailed information on the characterization of occupation probabilities, PAH uptake in the lung and skin, and daily working logs. It would be useful to characterize better the distribution of exposures by age of individuals exposed. Second, there is a need for sensitivity analysis using the Monte Carlo simulation model with the more detailed data sets as inputs. On the basis of the results of the sensitivity analysis, research should be directed to those parameters that, if better characterized, could most effectively reduce variability in the results.

5. Conclusions

Our work emphasizes the need to consider the nano and ultrafine particle-bound PAHs data in additional to genetic susceptibility and respiration data in order to obtain a more complete picture of factors influencing potential lung cancer risk caused by inhalation exposure to ambient PAHs. There were suggestions of an increased risk of lung cancer at the highest exposure levels of fine particle-bound PAHs. Our findings showed that predicted excess annual lung cancer incidence rate estimates ranged between 0.001 and 0.01 per 100,000 population, indicating no increase risk of lung cancer due to inhalation exposure to ambient PAHs in southern Taiwan. It is anticipated that the concept of *PAF* for limiting cumulative PAHs emissions to reduce lung cancer risk should play a prominent role in the future government risk assessment program. Better control program is afforded by a more thorough approach that combines an extensive database of nano/ultrafine particle-bound PAHs with a probabilistic assessment of their interpretive errors. The possible effects of long-term heavy inhalation exposure to ambient PAHs require further investigation.

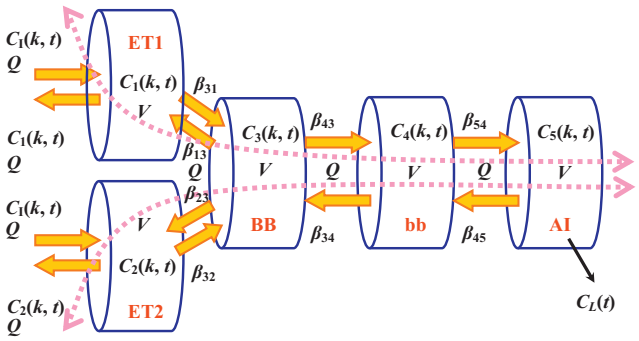

Fig. A1. The particle transport behaviors in human respiratory tract.

Appendix A. HRT model

Human respiratory system is divided into four anatomical regions, including (1) the extrathoracic region (ET), including ET1 and ET2, (2) the bronchial regions (BB), (3) the bronchiolar region (bb), and (4) the alveolar-interstitial regions (AI). The four regions also cover all other tissues in the human respiratory system, such as lymphatic tissue. Two main particle intake pathways are considered in human respiratory system: nasal (ET1) and oral (ET2). And the particles all deposit eventually in the following sequence: BB, bb, and AI during continuous breathing where the deposition mechanisms include gravitational settling, inertial impaction, interception, and diffusion in BB, bb and AI. The diagram of particle transport behavior in HRT was shown in Fig. A1 (Modified from [29]).

The general HRT model can be represented by a matrix form as [29,33],

$$\frac{dC(k,t)}{dt} = [L]\{C(t)\} + [B]\{u(k,t)\} \tag{A1}$$

where $\{C(k,t)\}=\{C_1(k,t), C_3(k,t), C_4(k,t), C_5(k,t)\}^T$ is the state variable vector of PAHs concentration in lung regions ET1, BB, bb, and AI, respectively (μg cm^{-3}); $\{u(k,t)\}=\{C_I(k,t)\,0\,0\,0\}^T$ represents an input vector of ambient PAHs concentration (ng cm^{-3}); $[L]$ (s^{-1}) is the state matrix containing size-specific transport rate coefficients of turbulent diffusive deposition rate, gravitational settling rate, and inertial impaction rate in each lung compartment as well as transition coefficients between lung compartments; and $[B] = \mathrm{diag}[Q/V_1, 0, 0, 0]$ (s^{-1}) is the constant input matrix where Q is the breathing rate (cm^3 h^{-1}) and V_1 is the volume of ET1 compartment (cm^3).

Appendix B. PBPK model

The general PBPK model can be written as follows,
Gas exchange compartment

$$C_{A1} = \frac{Q_C C_V + Q_P C_I}{Q_C + Q_P/P_B}, \tag{B1}$$

$$C_A = \frac{C_P}{P_P}, \tag{B2}$$

Lung compartment (where metabolism occurs)

$$V_P \frac{dC_P}{dt} = Q_C(C_{A1} - C_A) - \frac{V_{MAXP} C_A}{K_{MP} + C_A}, \tag{B3}$$

Liver compartment (where metabolism occurs)

$$V_L \frac{dC_L}{dt} = Q_L(C_A - C_{VL}) - \frac{V_{MAXL} C_{VL}}{K_{ML} + C_{VL}}, \tag{B4}$$

Other compartment

$$V_i \frac{dC_i}{dt} = Q_i(C_A - C_{Vi}), \tag{B5}$$

Venous return

$$C_V = \frac{Q_R C_{VR} + Q_F C_{VF} + Q_S C_{VS} + Q_L C_{VL}}{Q_C}, \tag{B6}$$

$$C_{Vi} = \frac{C_i}{P_i}, \tag{B7}$$

where C_{A1} is the concentration in blood leaving gas exchange compartment; C_A is the arterial blood concentration; C_I is the inhaled air concentration; C_P is the concentration in lung; C_L is the concentration in liver; C_{VL} is the concentration in venous blood leaving liver; C_i is the concentration in tissues i (richly perfused, fat, and slowly perfused); C_{Vi} is the concentration in venous blood leaving the tissues i; Q_P is alveolar ventilation rate; Q_C is cardiac output; Q_L is the blood flow rate to liver; Q_i is the blood flow rate to tissue i; P_B is the blood/air partition coefficient; P_P is the lung/blood partition coefficient; P_L is the liver/blood partition coefficient; P_i is the partition coefficient to tissue i; V_P is the lung volume; V_L is the liver volume; V_i is the tissue i volume; V_{MAXP} is the maximum metabolism velocity in lung; V_{MAXL} is the maximum metabolism velocity in liver; K_{MP} is the Michaelis constant of lung; and K_{ML} is the Michaelis constant of liver.

Appendix C.

Table C1
Physiological and biochemical parameters used in the human PBPK model.

Parameters	Human
Body weight (kg)	53.78–65.14
Alveolar ventilation rate ($L\,h^{-1}$)[a]	286.21–330.10
Cardiac output ($L\,h^{-1}$)[a]	286.21–330.10
Organ volumes (L)[a]	
Lung	1.24–1.50
Fat	12.62–15.29
Richly perfused tissues	1.99–2.41
Slowly perfused tissues	36.25–43.91
Liver	1.40–1.69
Blood flow rates ($L\,h^{-1}$)[a]	
Fat	14.31–16.51
Richly perfused tissues	145.97–168.35
Slowly perfused tissues	54.38–62.72
Liver	71.55–82.53
Partition coefficients[b]	
Blood:air	590
Lung:blood	1.37
Fat:blood	189.35
Richly perfused tissues:blood	12.47
Slowly perfused tissues:blood	7.36
Liver:blood	10.15
Metabolic constants[c]	
Maximum reaction rate in lung ($mg\,h^{-1}$)	0.104–0.119
Maximum reaction rate in liver ($mg\,h^{-1}$)	265.70–304.36
Michaelis constant of lung ($mg\,L^{-1}$)	0.06
Michaelis constant of liver ($mg\,L^{-1}$)	1.39

[a] Adopted from ICRP [46].
[b] Predicted values [36,37].
[c] Extrapolated values [47].

References

[1] J. Thyssen, J. Althoff, G. Kimmerle, U. Mohr, Inhalation studies with benzo alpha pyrene in Syrian golden-hamsters, J. Natl. Cancer Inst. 66 (1981) 575–577.
[2] R.P. Deutsch-Wenzel, H. Brune, G. Grimmer, Experimental studies on the carcinogenicity of five nitrogen containing polycyclic aromatic compounds directly injected into rat lungs, Cancer Lett. 20 (1983) 97–101.
[3] P. Boffetta, N. Jourenkova, P. Gustavsson, Cancer risk from occupational and environmental exposure to polycyclic aromatic hydrocarbons, Cancer Causes Control 8 (1997) 444–472.
[4] B. Armstrong, E. Hutchinson, J. Unwin, T. Fletcher, Lung cancer risk after exposure to polycyclic aromatic hydrocarbons: a review and meta-analysis, Environ. Health Perspect. 112 (2004) 970–978.
[5] J.P. Cheng, T. Yuan, Q. Wu, W.C. Zhao, H.Y. Xie, Y.G. Ma, W.H. Wang, PM_{10}-bound polycyclic aromatic hydrocarbons (PAHs) and cancer risk estimation in the atmosphere surrounding an industrial area of Shanghai, China, Water Air Soil Pollut. 183 (2007) 437–446.
[6] C.C. Lin, S.J. Chen, K.L. Huang, W.J. Lee, W.Y. Lin, J.H. Tsai, H.C. Chaung, PAHs, PAH-induced carcinogenic potency, and particle-extract-induced cytotoxicity of traffic-related nano/ultrafine particles, Environ. Sci. Technol. 42 (2008) 4229–4235.
[7] K. Ravindra, E. Wauters, R. Van Grieken, Variation in particulate PAHs levels and their relation with the transboundary movement of the air masses, Sci. Total Environ. 396 (2008) 100–110.
[8] B.G. Armstrong, G. Gibbs, Exposure-response relationship between lung cancer and polycyclic aromatic hydrocarbons (PAHs), Occup. Environ. Med. 66 (2009) 740–746.
[9] Y. Kawanaka, Y. Tsuchiya, S.J. Yun, K. Sakamoto, Size distributions of polycyclic aromatic hydrocarbons in the atmosphere and estimation of the contribution of ultrafine particles to their lung deposition, Environ. Sci. Technol. 43 (2009) 6851–6856.
[10] Y. Zhang, S. Tao, H. Shen, J. Ma, Inhalation exposure to ambient polycyclic aromatic hydrocarbons and lung cancer risk of Chinese population, Proc. Natl. Acad. Sci. U.S.A. 106 (2009) 21063–21067.
[11] Taiwan Department of Health (Taiwan DOH), Cancer Registry Annual Report, Taiwan DOH, Taiwan, 2007.
[12] H.H. Yang, S.O. Lai, L.T. Hsieh, H.J. Hsueh, T.W. Chi, Profiles of PAH emission from steel and iron industries, Chemosphere 48 (2002) 1061–1074.
[13] H.H. Yang, L.T. Hsieh, H.C. Liu, H.H. Mi, Polycyclic aromatic hydrocarbon emissions from motorcycles, Atmos. Environ. 39 (2005) 17–25.
[14] P.J. Tsai, T.S. Shih, H.L. Chen, W.J. Lee, C.H. Lai, S.H. Liou, Assessing and predicting the exposures of polycyclic aromatic hydrocarbons (PAHs) and their carcinogenic potencies from vehicle engine exhausts to highway toll station workers, Atmos. Environ. 38 (2004) 333–343.
[15] G.C. Fang, K.F. Chang, C.S. Lu, H.L. Bai, Estimation of PAHs dry deposition and BaP toxic equivalency factors (TEFs) study at Urban, Industry Park and rural sampling sites in central Taiwan, Taichung, Chemosphere 55 (2004) 787–796.
[16] G.C. Fang, Y.S. Wu, M.H. Chen, T.T. Ho, S.H. Huang, J.Y. Rau, Polycyclic aromatic hydrocarbons study in Taichung, Taiwan, during 2002–2003, Atmos. Environ. 38 (2004) 3385–3391.
[17] G.C. Fang, Y.S. Wu, P.P.C. Fu, I.L. Yang, M.H. Chen, Polycyclic aromatic hydrocarbons in the ambient air of suburban and industrial regions of central Taiwan, Chemosphere 54 (2004) 443–452.
[18] V.L. Colvin, The potential environmental impact of engineered nanomaterials, Nat. Biotechnol. 21 (2003) 1166–1170.
[19] G. Oberdorster, E. Oberdorster, J. Oberdorster, Nanotoxicology:, An emerging discipline evolving from studies of ultrafine particles, Environ. Health Perspect. 113 (2005) 823–839.
[20] A. Nel, T. Xia, L. Madler, N. Li, Toxic potential of materials at the nanolevel, Science 311 (2006) 622–627.
[21] N.L. Mills, K. Donaldson, P.W. Hadoke, N.A. Boon, W. MacNee, F.R. Cassee, T. Sandstrom, A. Blomberg, D.E. Newby, Adverse cardiovascular effects of air pollution, Nat. Clin. Pract. Cardiovasc. Med. 6 (2009) 36–44.
[22] D. Huh, B.D. Matthews, A. Mammoto, M. Montoya-Zavala, H.Y. Hsin, D.E. Ingber, Reconstituting organ-level lung functions on a chip, Science 328 (2010) 1662–1668.
[23] K.A. Bocskay, D. Tang, M.A. Orjuela, X. Liu, D.P. Warburton, F.P. Perera, Chromosomal aberrations in cord blood are associated with prenatal exposure to carcinogenic polycyclic aromatic hydrocarbons, Cancer Epidemiol. Biomarkers Prev. 14 (2005) 506–511.
[24] M. Ezzati, S. Vander Hoom, A. Rodgers, A.D. Lopez, C.D. Mathers, C.J.L. Murray, Comparative Risk Assessment Collaborating Group, Estimates of global and regional potential health gains from reducing multiple major risk factors, Lancet 362 (2003) 271–280.
[25] A.D. Lopez, C.D. Mathers, M. Ezzati, D.T. Jamison, C.J.L. Murray, Global and regional burden of disease and risk factors 2001 systematic analysis of population health data, Lancet 367 (2006) 1747–1757.
[26] S. Menzler, G. Piller, M. Gruson, A.S. Rosario, H.E. Wichrnann, L. Kreienbrock, Population attributable fraction for lung cancer due to residential radon in Switzerland and Germany, Health Phys. 95 (2008) 179–189.
[27] ICRP, Human Respiratory Tract Model for Radiological Protection, a Report of a Task Group of the International Commission on Radiological Protection, ICRP Publication No. 66, Pergamon Press, New York, 1994.
[28] M. Lazaridis, D.M. Broday, Ø.P.G. Hov, Georgopoulos, Integrated exposure and dose modeling and analysis system. 3. Deposition of inhaled particles in the human respiratory tract, Environ. Sci. Technol. 35 (2001) 3727–3734.

[29] J.W. Chen, C.M. Liao, S.C. Chen, Compartmental human respiratory tract modeling of airborne dust exposure from feeding in swine buildings, J. Air Waste Manage. Assoc. 54 (2004) 331–341.
[30] J.E. Dennison, M.E. Anderson, H.J. Clewell, R.S.H. Yang, Development of a physiologically based pharmacokinetic model for volatile fractions of gasoline using chemical lumping analysis, Environ. Sci. Technol. 38 (2004) 5674–5681.
[31] H.J. Clewell, P.R. Gentry, J.E. Kester, M.E. Anderson, Evaluation of physiologically based pharmacokinetic models in risk assessment: an example with perchloroethylene, Crit. Rev. Toxicol. 35 (2005) 413–433.
[32] C.M. Liao, S.C. Chen, A probabilistic modeling approach to assess human inhalation exposure risks to airborne aflatoxin B1 (AFB1), Atmos. Environ. 39 (2005) 6481–6490.
[33] C.M. Liao, J.W. Chen, S.J. Huang, Size-dependent PM10 indoor/outdoor/personal relationships for a wind-induced naturally ventilated airspace, Atmos. Environ. 37 (2003) 3065–3075.
[34] M.E. Andersen, H.J. Clewell, M.L. Gargas, F.A. Smith, R.H. Reitz, Physiologically based pharmacokinetics and the risk assessment process for methylene chloride, Toxicol. Appl. Pharmacol. 87 (1987) 185–205.
[35] H. Mielke, A. Gundert, K. Abraham, U. Gundert-Remy, Acute inhalative exposure assessment: derivation of guideline levels with special regard to sensitive subpopulations and time scaling, Toxicology 214 (2005) 256–267.
[36] P. Poulin, K. Krishnan, A biologically-based algorithm for predicting human tissue-blood partition coefficients of organic chemicals, Hum. Exp. Toxicol. 14 (1995) 273–280.
[37] P. Poulin, F.P. Theil, Prediction of pharmacokinetics prior to in vivo studies. 1. Mechanism-based prediction of volume of distribution, J. Pharm. Sci. 91 (2002) 129–156.
[38] J.C. Ramsey, M.E. Andersen, A physiologically based description of the inhalation pharmacokinetics of styrene in rats and humans, Toxicol. Appl. Pharmacol. 73 (1984) 159–175.
[39] L.S. Goldstein, To BaP or not to BaP? That is the question, Environ. Health Perspect. 109 (2001) A356–A357.
[40] T.I.C. Nisbet, P.K. LaGoy, Toxic equivalency factors (TEFs) for polycyclic aromatic hydrocarbons (PAHs), Regul. Toxicol. Pharmacol. 16 (1992) 290–300.
[41] D. Mirabelli, An improved estimate of the quantitative relationship between polycyclic hydrocarbons and lung cancer, Occup. Environ. Med. 66 (2009) 716–717.
[42] A.G. Russell, B. Brunekreef, A focus on particulate matter and health, Environ. Sci. Technol. 43 (2009) 4620–4625.
[43] S. Bae, X.C. Pan, S.Y. Kim, K. Park, Y.H. Kim, H. Kim, Y.C. Hong, Exposures to particulate matter and polycyclic aromatic hydrocarbons and oxidative stress in schoolchildren, Environ. Health Perspect. 118 (2010) 579–583.
[44] I. Mordukhovich, P. Possner, M.B. Terry, R. Santella, Y.J. Zhang, H. Hibshoosh, L. Memeo, M. Mansukhani, C.M. Long, G. Garbowski, M. Agrawal, M.M. Gaudet, S.E. Steck, S.K. Sagiv, S.M. Eng, S.L. Teitelbaum, A.I. Neugut, K. Conway-Dorsey, M.D. Gammon, Associations between polycyclic aromatic hydrocarbon-related exposures and p53 mutations in breast tumors, Environ. Health Perspect. 118 (2010) 511–518.
[45] S. Tao, D. Zhang, Y. Lu, L. Li, J. Ding, Y. Yang, Y. Yang, X. Wang, W. Liu, B. Xing, Mobility of polycyclic aromatic hydrocarbons in the gastrointestinal tract assessed using an in vitro digestion model with sorption rectification, Environ. Sci. Technol. 44 (2010) 5608–5612.
[46] ICRP, Basic Anatomical and Physiological Data for Use in Radiological Protection: Reference Values, ICRP Publication No. 89, Pergamon Press, New York, 2003.
[47] D.A. Wiersma, R.A. Roth, The prediction of benzo[*a*]pyrene clearance by rat liver and lung from enzyme kinetic data, Mol. Pharmacol. 24 (1983) 300–308.